A Flexible Subcarrier Multiplexing System With Analog Transport and Digital Processing for 5G (and Beyond) Fronthaul

Shabnam Noor, *Student Member, IEEE*, Philippos Assimakopoulos, *Member, IEEE*, and Nathan J. Gomes, *Senior Member, IEEE*

***Abstract*—A flexible subcarrier multiplexing system combining analog transport with digital domain processing is presented. By making use of bandpass sampling and applying a systematic mapping of signals into available Nyquist zones, the multiplexing system is able to present multiple signals at the same intermediate frequency at the remote site. This simplifies the processing required for multiple antenna systems. We further propose the use of track-and-hold amplifiers at the remote site. These elements are used to extend the mapping to a mapping hierarchy, offering flexibility in frequency placement of signals and relaxation of analog-to-digital converter bandwidth and sampling rate constraints. The system allows the transport of different numerologies in a number of next generation radio access network scenarios. Experimental results for large signal multiplexes with both generic and 5th-generation mobile numerologies show error-vector magnitude performance well within specifications, validating the proposed system. Simulation results from a system model matched to these experimental results provide performance predictions for larger signal multiplexes and larger bandwidths.**

***Index Terms*—Digital signal processing, massive-MIMO (mMIMO), millimeter wave (mmW), mobile fronthaul, radio-over-fiber, subcarrier multiplexing (SCM).**

I. Introduction

THE establishment of heterogeneous networking and multi-antenna techniques as norms for next generation radio access networks (RANs) means that new network architectures will need to be employed that can seamlessly accommodate such features. These architectures will have to meet differing requirements in terms of data rate, latency constraints, system complexity and cost.

Analog transport within the fronthaul, as an alternative to digital transport based either on centralized processing with the Common Public Radio Interface (CPRI) [1], or on alternative functional decompositions [2], [3], can provide high spectral efficiency and reduced latency, allowing joint processing of signals at the Distributed Unit (DU). Therefore, there is renewed interest in the use of analog Radio over Fiber (RoF) techniques in next generation mobile networks [4]–[7].

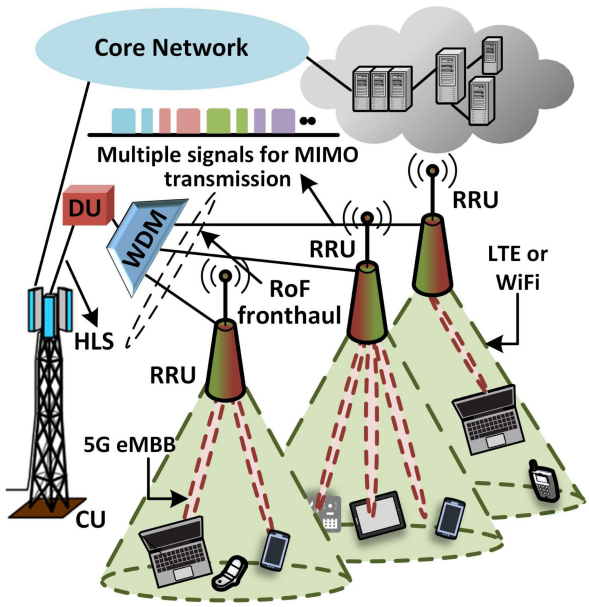

Fig. 1. 5G Heterogeneous Network Configuration. CU, Central Unit; RRU, Remote Radio Unit; HLS, Higher Layer Split; DU, Distributed Unit; WDM, Wavelength Division Multiplexing; RoF: Radio over Fiber; MIMO, Multiple-Input Multiple-Output; eMBB, Enhanced Mobile Broadband; LTE, Long Term Evolution.

A concept diagram for an analog fronthaul for 5th generation mobile (5G) networks is shown in Fig. 1. Here signals originating from a core network are received by a decomposed base station comprising of a Central Unit (CU), a Distributed Unit (DU) and Remote Antenna Units (RRUs). The DU performs all the processing for different numerologies (the term numerology is used here in a generalized manner to describe Orthogonal Frequency Division Multiplexing (OFDM) signals with different generation characteristics, and does not refer specifically to 5G signals). After that, the signals are combined through Subcarrier Multiplexing (SCM) with analog transport to RRUs. Different RRUs may then be addressed by different wavelengths using Wavelength Division Multiplexing (WDM). Sub-6 GHz WiFi or LTE signals can be used to provide wider area coverage while

Manuscript received March 5, 2019; revised April 18, 2019; accepted May 15, 2019. Date of publication May 22, 2019; date of current version July 17, 2019. The work of P. Assimakopoulos was supported in part by the project NIRVANA (EP/L02603/1) under the EPSRC's "Towards an Intelligent Information Infrastructure (TI3)" program and in part by the EU Horizon 2020 5G-DRIVE project under Grant 814956. *(Corresponding author: Shabnam Noor.)*

The authors are with the Communications Research Group, University of Kent, Canterbury CT2 7NT, U.K. (e-mail: s.noor@kent.ac.uk; p.asimakopoulos@kent.ac.uk; n.j.gomes@kent.ac.uk).

Color versions of one or more of the figures in this paper are available online at http://ieeexplore.ieee.org.

Digital Object Identifier 10.1109/JLT.2019.2918215

5G millimeter-wave (mmW) signals use narrow beams through beamforming.

Traditional SCM techniques rely on analog components to multiplex signals and thus lack scalability (in terms of cost and complexity) for wide bandwidth and large size multiplexes [8]–[11]. Digital multiplexing techniques, on the other hand, are promising, but must be as flexible and scalable as possible to operate within a dynamic next generation mobile network (5G and beyond) that includes different numerologies and bandwidths, multiple antenna techniques and heterogeneous networking (HetNet). Flexibility is of prime importance in such a network, requiring the SCM transport architecture to be able to dynamically adapt to accommodate such differing use cases.

Multiplexes occupying large bandwidths would normally require equally large sampling rates at the RRUs, and Analog-to-Digital Converters (ADCs) with sufficiently large analog bandwidths [6], [7], [12], [13]. A traditional approach to reducing sampling rates is to employ band-pass sampling [14]. In [15], band-pass sampling has been used in conjunction with analog domain filtering to de-multiplex a large number of signals, showing that low sampling rate ADC-induced aliasing effects can be rectified by MIMO processing. In [16], a low sampling rate ADC was used to frequency translate a millimeter Wave (mmW) signal to Radio Frequency (RF) in the uplink section of a digitized fronthaul, while in [17], a track-and-hold amplifier (THA) was used at the transmitter side of a fronthaul link to band-pass sample a signal down to baseband.

However, prior work has not considered the signal placement in the RRU either in the digital or analog domain, especially when large numbers of signals are transmitted for mMIMO and/or in multi-RAT applications. Individual signals may reside at different IFs, thus up-conversion stages to RF/mmW need to be bespoke, adaptable for each signal, and frequency/phase synchronized. Therefore, a flexible technique for obtaining all signals at the same Intermediate Frequency (IF), thereby reducing the amount of per-signal processing at the RRU, would be beneficial. Furthermore, architectures such as the one presented in [15] would require a very large number of analog filters for filtering individual signals or small groups of signals (for example, 128 filters for 128 signals with filtering for each, or 64 filters when filtering pairs of signals). As this filtering is carried out in the analog domain, no flexibility is provided in adapting these filters and the number of signals they each filter. Therefore, an approach that is more flexible and not affected by signal counts would be beneficial.

In this paper, such issues are addressed by employing a systematic single-Inverse Fast Fourier Transform (IFFT)-aided mapping into Nyquist zones (NZs) that ensures that signals are obtained at the same IF at the RRU by using a single down-sampling factor and allowing these signals to be readily up-converted to their respective RF/mmW frequencies. Moreover, both Discrete Multi-tone (DMT) signals, which have found widespread use in Optical-Wireless Communications (OWC) [18], [19] and Single Sideband Modulation (SSB) signals, are multiplexed seamlessly and efficiently using the single IFFT operation. Furthermore, for multiplexes with large aggregate bandwidths or residing at high IF/RF frequencies, ADCs with very high analog bandwidths (e.g., in excess of 10 GHz in [15]) would be required, making such systems very expensive. Therefore, a reduction of the analog bandwidth constraints of RRU ADCs is very important. To this end, we propose the use of Track-and-Hold Amplifiers (THAs) at the RRU side and as such, tackle the ADC analog bandwidth limitations at the RRU. Previously, there has been limited proposed use of THAs in RoF applications, for example in [20], and here on the transmitter side of a digital link.

The paper is organized as follows: Section II presents the mapping and multiplexing design concept while Section III presents the system architecture, separated into the signal processing and subcarrier multiplexing part, and mmW generation part. Section IV presents measurement results, while Section V presents a model of the system matched with measurement results with generic and 5G numerologies, and performance predictions with a THA. The paper is concluded in Section VI.

II. Signal Multiplexing and Nyquist Zone Mapping Technique Concepts

A conceptual view of the multiplexing and mapping techniques and how they relate to the different DU and RRU processes is shown in Fig. 2, while more detailed descriptions of individual processes are provided within Figures 3 to 6. Fig. 2 shows that at the DU side, channel multiplexes are created in the frequency domain while a single-IFFT stage operation is used to convert the composite channel structure into the time domain. Note that the implicit assumption here is that within the DU, frequency domain samples are directly available, and it is on these samples that the next stages of processing (mapping and multiplexing), described in the following paragraphs, take place.

The technique of creating the multiplex and seamlessly integrating SSB- and DMT-derived channels using a single-IFFT stage operation is shown in more detail in Fig. 3. The IFFT employs a sampling rate of $f_{s,ifft}$ giving rise to two NZs with a width of $f_{s,ifft}/2$. The channels are organized groupings of contiguous modulation mapping-derived (e.g., QAM, QPSK, BPSK etc.) frequency domain samples. Such contiguous samples are separated by arbitrary numbers of null samples, which facilitate digital filtering at the receiver side. The null samples are essentially frequency guard bands. The channels are distributed in both NZs (each with a size of $f_{s,ifft}/2$) such that they are symmetric in their number of frequency domain samples across the two NZs and where:

1) The DMT-derived channels are created such that corresponding channels in the two NZs are conjugate symmetric, leading to a theoretical maximum number, *n*, of DMT channels.
2) The SSB-derived channels are created such that corresponding groupings in the two NZs are not conjugate symmetric, leading to a theoretical maximum number *2n*, of SSB-derived channels.

With this technique, there is no need for analog or digital domain filters (for removing sidebands) or Hilbert transforms (typically used to create SSB signals). Note that processes prior to the IFFT are in the "frequency domain" while following the

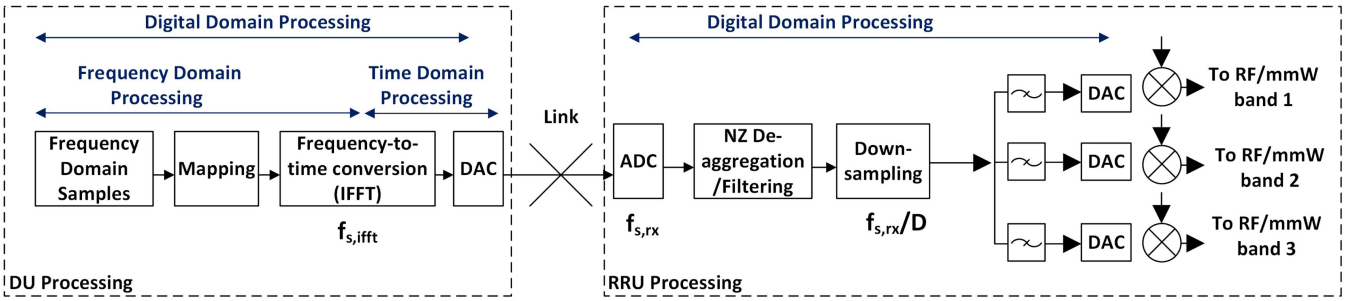

Fig. 2. Conceptual view of the multiplexing and mapping techniques and how they relate to the different DU and RRU processes.

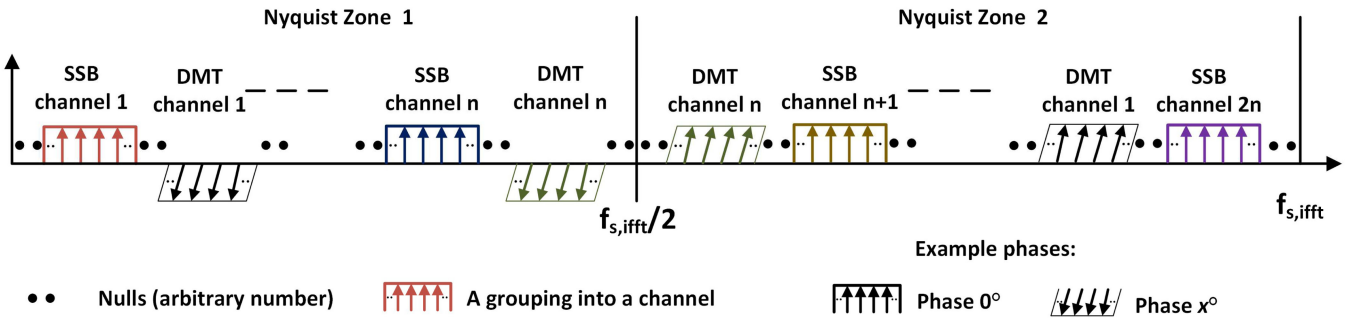

Fig. 3. The multiplexed channel structure at the input of the IFFT processing stage that would take place at the transmitter side (DU) showing the two IFFT-derived NZs.

IFFT, the resulting signal and remaining processes are said to be in the "time domain".

The channels can be made of groupings of different numbers of frequency domain samples giving rise to different bandwidth channels, but have the same spacing between adjacent frequency samples. For illustration purposes, in Fig. 3, the SSB- and DMT-derived channels are shown as interleaved. However, any possible combination and/or placement of DMT and SSB-derived channels can be employed. Also to simplify the description, a common phase for all the frequency domain samples (that make up each channel) is shown here, but in reality, each sample will have its own phase as determined by the modulation mapping (real or complex) and the relative amplitudes of the In-phase and Quadrature components that make up each sample. When the channels across the two NZs are not conjugate symmetric (this will be the case when DMT and SSB channels are multiplexed or when solely SSB channels are multiplexed) the IFFT output is complex, necessitating the use of quadrature processing in the following stages (e.g., dual DACs).

The two NZs (with a size of $f_{s,ifft}/2$) shown here are derived by the sampling rate of the IFFT operation. However, mapping of channels into specific locations within the channel multiplex is carried out in a systematic manner such that all channels fall within specific locations within NZs derived by the down-sampling operation carried out at the RRU. That is, channels that make up the multiplex, are placed at appropriate frequency domain locations prior to the single-IFFT stage operation, while the placement (i.e., precise IF of each signal) is carried out in such a way that individual or groups of channels are mapped into separate RRU-derived NZs and placed in specific positions within them. In Fig. 4, examples of different channel mappings per RRU-derived NZs are shown. As stated previously, the channels combined within a NZ may have any/different bandwidth(s), although they are illustrated as having the same bandwidth for simplicity. Channels that occupy the same NZ form a "channel group". Note that the first NZ, as derived by the IFFT operation at the DU with a size of $f_{s,ifft}/2$, is also depicted at the top of Fig. 4 for reference.

Each RRU-derived NZ has a size given by $F_{s,rx}/2$, where

$$F_{s,rx} = f_{s,rx}/D \text{ for } D \in \mathbb{N}^+, \tag{1}$$

and $f_{s,rx}$ is the sampling rate of the ADC at the RRU side while D is the down-sampling factor used in the succeeding down-sampling stage. D is not chosen arbitrarily, it instead depends on the number of channels within each multiplex. The sampling rate of the ADC in this example is larger than or equal to the sampling rate of the IFFT at the transmitter side but this need not be the case. (Support for higher sampling rates at the DU, larger than the ADC's sampling rate, will be described later in Section V.) As the sampling rate $(F_{s,rx})$ at the RRU is smaller than $f_{s,rx}$, the result is the creation of NZs with mirror images around every multiple of $F_{s,rx}/2$ ($F_{s,rx}/2$, $F_{s,rx}$, $3F_{s,rx}/2$ and so on). This means that the frequency spectrum is divided into a (theoretically) infinite number of NZs, each having a width equal to $f_{s,rx}/(2D)$. Making use of this, an arbitrary number of channels can be located within each NZ provided that the total bandwidth they occupy is smaller than $f_{s,rx}/(2D)$ (that is the Nyquist criterion is met). The number of NZs and their bandwidth depend on the ADC sampling rate and the down- sampling factor to be used at the RRU. (Later, in

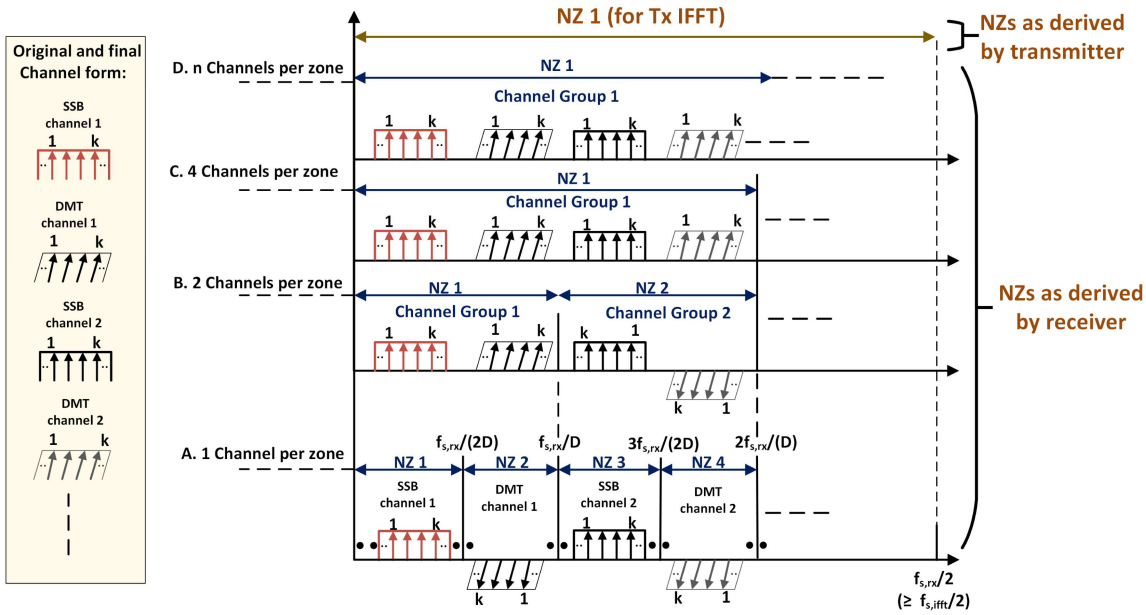

Fig. 4. The mapping technique that would take place at the transmitter side (DU) showing an example of four channel mapping cases (A to D).

Section V, we will show how the mapping can be extended to a hierarchy where the THA parameters will also be taken into account in the determination of a second "level" of NZs).

Fig. 4, shows examples of channel mappings, with one channel per NZ up to n channels per NZ. If we consider M to be the total number of channels in the positive part of the spectrum and N to be the number of NZs, the number of channels in each NZ (i.e., the size of the channel group) is given as

$$m = \frac{M}{N} \text{for } M, N \in \mathbb{N}^+ \ \& \ N \leq M. \tag{2}$$

Channels that are in even NZs are pre-processed at the DU side in order to reduce the processing required at the RRU side. This processing is carried out per NZ, that is, on individual channels or channel groups when individual or groups of channels occupy even-order NZs.

This processing conjugates and frequency flips these channels. Then, following the down-sampling process at the RRU, the channels are obtained back in their original form. Which channels or channel groupings will occupy which order NZs will depend on how individual channels are mapped and whether the multiplex is up-converted to an RF frequency at the input of the link. For example, for the four channels annotated in Fig. 4, for Case A, with one channel per NZ, DMT channel 1 and DMT channel 2 are pre-processed in the described manner while SSB channel 1 and SSB channel 2 are not. For Case B, with two channels per NZ, DMT channel 1 and SSB channel 1 are not pre-processed while DMT channel 2 and SSB channel 2 are. For Case C with four channels per NZ, the four channels shown on the Figure are not pre-processed (the next four channels, not annotated on the Figure, would be pre-processed). Note that for Case A (one channel per NZ), direct down-conversion to baseband is possible by mapping each channel across the boundary of each NZ. In such a case, frequency pre-flipping and pre-conjugation can be avoided. However, this is only a special case (and specific to mapping one channel per NZ) that may not make efficient use of the available bandwidth offered by each NZ, especially when channels with different bandwidths need to be multiplexed.

Following the mapping and IFFT processes, the multiplex is converted into the analog domain by a DAC process. Note that prior to or following this stage, the output of several single-IFFT stage processed blocks can be combined to create a composite multiplex. This process is shown in Fig. 5. Each frequency domain multiplex that is sent to a single-IFFT stage has areas devoid of channels by the appropriate insertion of null samples. These unoccupied areas can readily allow the insertion of channels from other single-IFFT stage processed multiplexes. The combining process can be carried out either in the digital domain, prior to the DAC, by appropriate interpolation and/or decimation of each single-IFFT stage output, or in the analogue domain, following the DAC, using a simple RF combiner. The combining process, depicted in Fig. 5, of several single-IFFT stage outputs is carried out in the time domain (discrete or continuous) and is akin to traditional power combining carried out in optical-SCM systems [4], [10]. Significantly, the different single-IFFT stage outputs can be created with different sampling rates allowing different OFDM numerologies to be combined.

In general, employing large IFFTs may increase computation complexity compared to multiple small IFFTs (the traditional method of generating multiple OFDM signals) but the increase is not large as it increases little more than linearly. Furthermore, other processes relating to the multiplexing operation of the individual IFFT outputs (e.g., digital/analog up-converters) may balance out the complexity increase and this is the subject of ongoing work. Still, if there is a requirement to reduce IFFT sizes, the mapping technique described here, can be employed through a combination of several reduced-size single-IFFT stage outputs

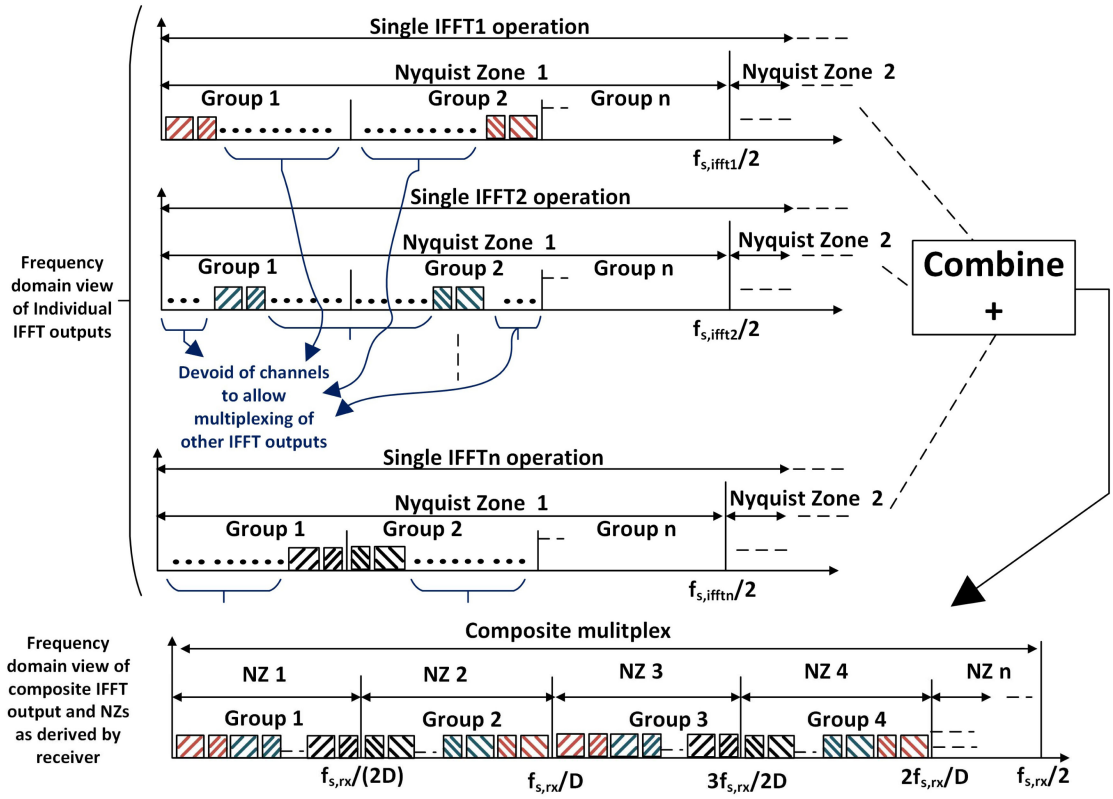

Fig. 5. Conceptual view of the process of combining several single-IFFT stage outputs into a composite multiplex by creating areas devoid of channels in each individually single-IFFT processed block.

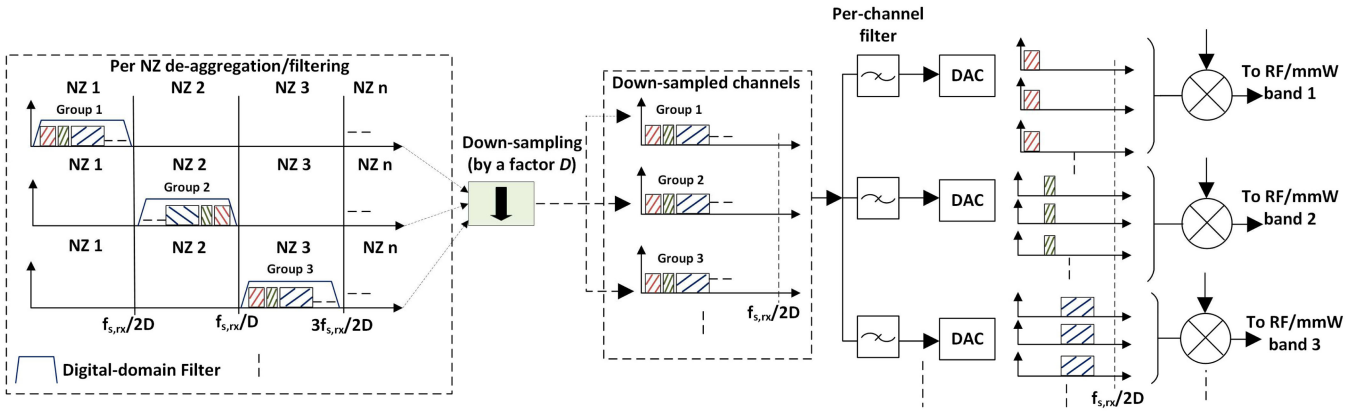

Fig. 6. Conceptual view of receiver side (RRU) processing following the ADC stage, consisting of per-NZ digital domain de-aggregation/filtering, down-sampling, per-channel digital domain filtering, digital-to-analog conversion and up-conversion to RF/mmW bands.

(using the technique described in Fig. 5 if channels of different numerologies need to be multiplexed) followed by appropriate digital up-conversion stage(s).

The composite multiplex is then transmitted over a link. At the RRU side the received multiplex is converted directly into the digital domain by an ADC process (note that in practical applications a wide-bandwidth filter may be required prior to the ADC). Following this, each channel group within each NZ is de-aggregated by digital filters. Then, a down-sampling process frequency translates each channel group down to the same IF frequency.

Fig. 6 shows a more detailed view of these processes. To avoid aliasing, the RRU must include some processing to de-multiplex the signals prior to down-sampling. To this end, a digital filter bank is used to filter channel groups within NZs. Following this stage, band-pass sampling is performed with a common factor, D, resulting in a sampling rate of $f_{s,rx}/D$ whereby mirror images of each channel group are created within each NZ having a width of half of this rate $f_{s,rx}/(2D)$. Significantly, a copy of the channel group is created in the first NZ. All channel groups have now been frequency translated down to the same IF without the use of additional analog/digital mixers.

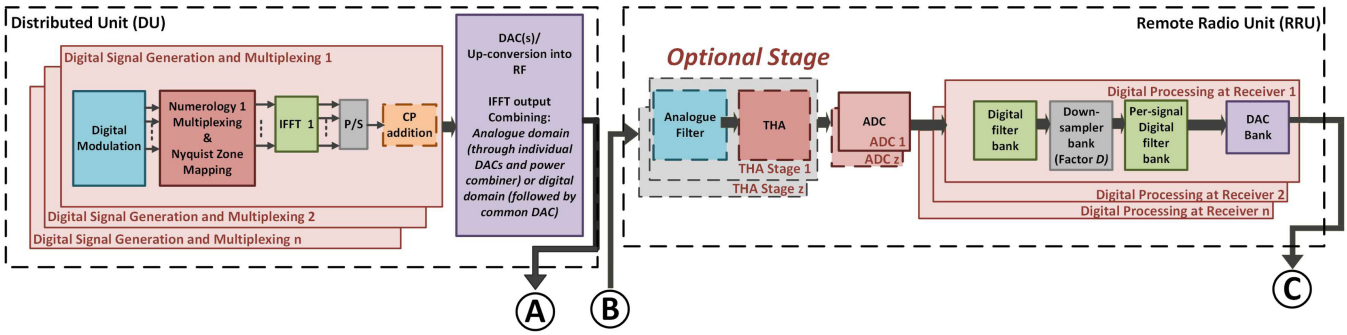

Fig. 7. Digital signal generation and subcarrier multiplexing at transmitter (DU) and digital processing at receiver (RRU). QAM, Quadrature Amplitude Modulation; IFFT, Inverse Fast Fourier Transform; CP, Cyclic Prefix; DAC, Digital-to-Analog Converter; THA, Track-and-Hold Amplifier; ADC, Analog-to-Digital Converter.

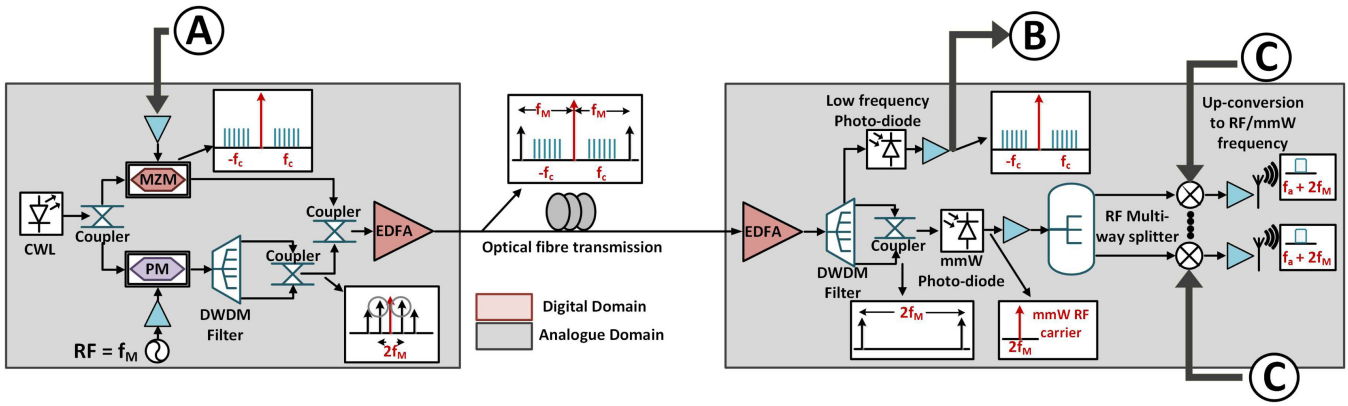

Fig. 8. Data modulation and remote LO delivery via optical frequency comb generation for mmW up-conversion. CWL, Continuous Wave Laser; PM, Phase Modulator; DWDM, Dense Wavelength Division Multiplexing; MZM, Mach-Zehnder Modulator; EDFA, Erbium Doped Fiber Amplifier; mmW, Millimeter Wave.

The channels within each channel group may have been generated using different numerologies (for example, combined with the process described in Fig. 5) and may be destined to the same or different RF/mmW channels (e.g., in multi radio access technology (multi-RAT) transmission, incorporating a 5G mmW signal and a sub-6 GHz Wi-Fi or LTE signal with narrower bandwidth. Thus, following the down-sampling process, individual channels within each channel group are filtered with digital filters and are converted back into the analog domain using a DAC. At this stage, channels within each channel group that are at the same IF can be readily up-converted to their respective RF/mmW band without the need for additional digital or analog frequency translation processes.

III. System Architecture

A detailed overview of the proposed architecture that performs the processes described in Section II is shown in Fig. 7. The digital multiplexing processes are elaborated in Subsection III.A. The data modulation and mmW carrier generation parts of the architecture are presented in Fig. 8 and elaborated in Subsection III.B. To aid the description, in the following sections the term "signal(s)" will be used interchangeably with "channel(s)" for both frequency domain and time domain channel representations.

A. Signal Processing and Subcarrier Multiplexing Using DMT and SSB Modulation

Multiple signals (these can have different modulation formats) are generated and multiplexed in the frequency domain as shown in Fig. 7. Pilots are inserted at known locations of a QAM symbol sequence for tracking changes in the channel response (not shown in Fig. 7). This is followed by frequency domain pre-conjugation and pre-flipping of the signals that will occupy even NZs, processes that are reversed by the down-sampling stage at the receiver.

As described in Section II, frequency guard bands in the form of null samples are added between the QAM sample groupings in order that separate signals and signal groups are created (as required) in the frequency domain (prior to the the single-IFFT operation). In addition, when the outputs of several single-IFFT stages are multiplexed, such guard bands are also used to create gaps where signals generated by other IFFTs can be inserted in accordance with the process described in Fig. 5. Note that the architecture allows for variable/arbitrary signal bandwidths and frequency gaps between signals, and combines both DMT and SSB signals flexibly and seamlessly within a single-IFFT stage.

Following the IFFT stage, a Cyclic Prefix (CP) is appended to each multiplex and the signals are sent to a DAC and up-conversion to RF stage. Note, that in this implementation, the

composite radio waveform is generated at the DU with the CP included. In this way, following the de-multiplexing and down-sampling processes at the RRU side, each individual signal will directly have its own decimated and appropriately sized CP and can thus be directly processed for transmission over the wireless channel. However, as the CP is principally for Inter-symbol Interference (ISI) mitigation over the wireless channel (in addition to simplifying equalization at the user equipment), it could be generated at the RRU. This would save some bandwidth over the RoF link, at the expense of extra processing for CP addition at the RRU.

The final multiplex is then modulated onto an optical carrier using a Mach-Zehnder Modulator (MZM).

At the RRU side, after being detected by a low-frequency photodiode (PD), the signals are sent to an optional analog filter-Track-and-Hold Amplifier stage (the operation of the THA will be discussed in Section V) or directly to a ADC. The signals are then processed in the manner described in Section II: signal(s) in each resulting NZ are filtered using a digital filter bank and band-pass sampled, using a common sampling rate, down to the first NZ. The resulting signals within each NZ are individually filtered, and sent to the appropriate DAC and up-conversion stages.

B. Data Modulation and mmW Carrier Generation

As shown in Fig. 8, at the DU, the optical signal from a Continuous Wave Laser (CWL) is split using an optical coupler/power divider. One part is modulated by the subcarrier multiplex using an MZM. The signal multiplex is placed at an RF of f_c. The second part of the CWL signal is phase-modulated by a Phase Modulator (PM), which produces optical sidebands with a separation equal to the modulation frequency of the RF signal applied (f_M). The first order sidebands are filtered using a Dense Wavelength Division Multiplexing (DWDM) filter and then coupled with the data-modulated signals from the MZM. The resulting signal is optically amplified and transmitted through the optical fiber link.

At the RRU, the signals are sent to another DWDM filter. The optical carrier with the data-modulated signals is filtered and sent to a low-frequency PD. Following the optical to electrical conversion, the signal multiplex is digitized for the subsequent digital processing stage (discussed in subsection A).

At the same time, the optical sidebands, separated by a frequency of $2f_M$ are detected by a mmW PD to produce a mmW beat signal. The mmW signal is then distributed (through appropriate splitters) to up-conversion stages where the individual signals of the SCM multiplex are up-converted to a frequency of $f_a + f_M$ for mmW-mMIMO transmission, f_a being the IF of the down-sampled signal.

IV. Experimental Results

Due to equipment limitations, some modifications have been made in the experimental setup compared to diagram shown in Fig. 8. Separate fibers have been used for the transport of signal multiplexes and the sidebands for mmW up-conversion (thus, the DWDM filter in the RRU in Fig. 8 is not required). Only one Erbium Doped Fiber Amplifier (EDFA) was used and due to power limitations in the setup, the RF multi-way splitter has not been used. For simplicity, the first NZ of the digital multiplex has been left unoccupied. Lastly, the functions of the THA-ADC have been performed by a real-time oscilloscope. The outputs at different stages of the architecture (points A – C, corresponding to the same points in Figures 7 and 8) are shown in Fig. 9.

For performance verification, initially, a generic numerology and frequency spacing is used to produce 64 SSB/DMT signals, with OFDM subcarrier modulation using 16-QAM. The subcarrier multiplex is produced in MATLAB using the Nyquist zone mapping method, with the resulting spectrum shown in Fig. 9A. The multiplex is downloaded to a Tektronix AWG7122C Arbitrary Waveform Generator (AWG), which up-converts it to an RF frequency (f_c) of 1.56 GHz.

For simplicity, the sampling rate set at the AWG has to be at least 1.25 times the aggregate bandwidth of the signal (this is so that the AWG and Oscilloscope operate at the same sampling rate). To meet this requirement, 14 out of 64 SSB signals (7 in each of the "positive" and "negative" part of the spectrum) are replaced by null subcarriers. Considering that the signal in the first NZ is also replaced by null subcarriers, a total of 48 signals are transmitted. A sampling rate of 3.13 GSps (the maximum practically allowed by the AWG) and an IFFT length of 32768 are used, leading to a bin size of 95.37 kHz. This results in a bandwidth per signal of 38.15 MHz, a gap of 10.68 MHz between signals and a total bandwidth of approximately 2.42 GHz being occupied by the multiplex. Using solely DMT modulation, the maximum aggregate data rate is 3.66 Gbps, while for SSB modulation it is 7.32 Gbps. It should be noted that the particular gap between the signals has been chosen to aid mmW up-conversion. Again, this is done to maintain the bandwidth to sampling rate ratio of 1.25. Potentially, this gap can become arbitrarily small if digital filters with sufficient selectivity can be used at the RRU.

As shown in Fig. 8, at the DU, one part of the optical carrier is intensity modulated by the up-converted multiplex, with an MZM biased at an optimum working point between quadrature and null [4]. The resulting spectrum (one-sided) at the output of the photodiode at the RRU is shown in Fig. 9B; the roll-off at higher frequencies is a result of the AWG's sinc-type amplitude response [21]. The multiplexed signals are captured by a Tektronix DPO72304DX Real-Time Digital Phosphor Oscilloscope and processed offline by a MATLAB receiver function that applies the digital domain processes described in Section II and III.A. The constellation diagrams of Signals 2, 11, 18 and 25 of the multiplex are shown in Fig. 9C. Signal 2 is the first signal of the multiplex while Signal 25 is the last signal of the multiplex and signals 11 and 18 have been chosen to represent the middle region of the multiplex. The range of EVM results is from 4% for signals at lower frequencies to 7% for signals closer to 4 GHz, showing EVM performance well within the 3rd Generation Partnership Project (3GPP) specification limit of 12.5% for 16-QAM [22]. The worse performance for the signals at higher frequencies is a result of the AWG's amplitude response. Of these signals, the first and last signals in the multiplex (signals 2 and 25) are chosen for mmW up-conversion and

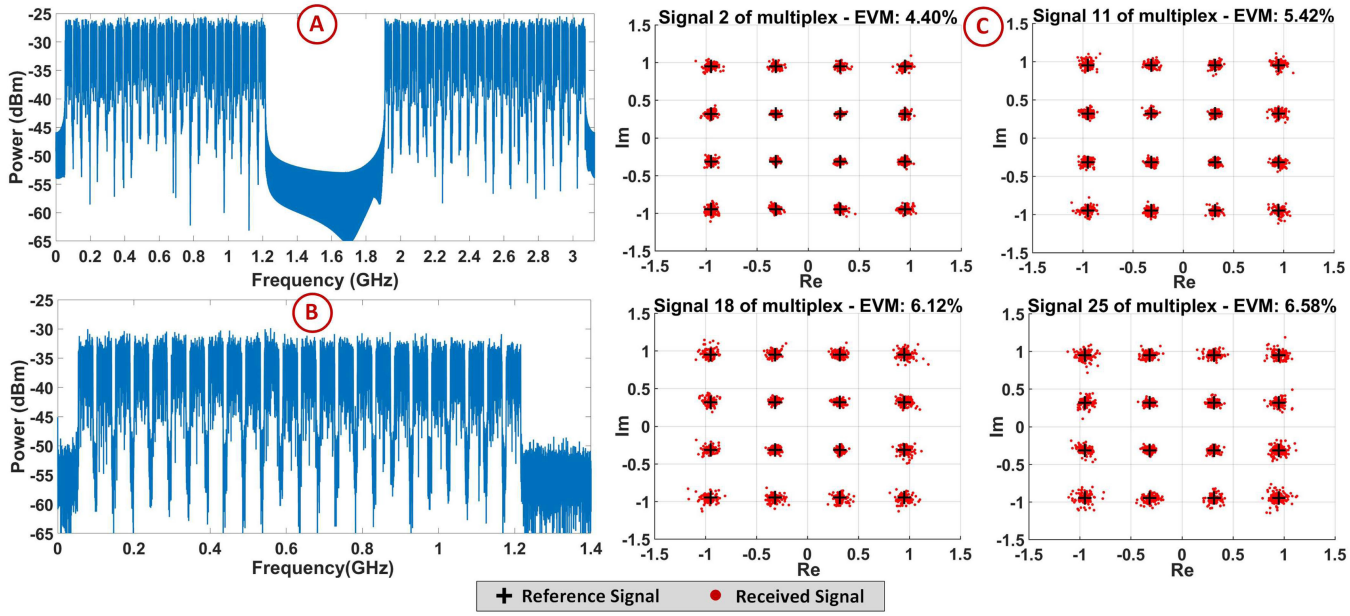

Fig. 9. A. Transmit spectrum of 64 SSB/DMT signal multiplex as seen in MATLAB; B. Received spectrum (one-sided) at the oscilloscope; C. EVM/ constellation diagrams of Signals 2, 11, 18 and 25 of multiplex (corresponding to points A, B and C of Fig. 7).

are extracted and downloaded back into the AWG. Each signal is then regenerated at an arbitrary IF, using a sampling rate of approximately 97.66 MSps (i.e., the original F_s has been decimated by a factor of 32). The remotely delivered mmW carrier is used to up-convert the digitally processed signals. Double sidebands are produced due to the mmW up-conversion and a narrowband band-pass filter centered at 26.3 GHz is used to filter out the required upper sideband. However, this filtering stage can be avoided by using a mmW quadrature mixer. Finally, following transmission over a short-length co-axial cable, the signals are down-converted and recaptured with the real-time oscilloscope for performance evaluation. The received spectra and the constellations, following OFDM demodulation corresponding to Signals 2 and 25 are shown in Fig. 10. The EVM for Signals 2 and 25 are 8.8% and 8.5%, respectively, and are again well within 3GPP limits [22].

V. 5G Numerology and Simulation Predictions

The experimental setup shown in Figures 7 and 8 has been modeled in a MATLAB-Virtual Photonics Inc. (VPI) co-simulation environment. Similarly to the experimental process described in Section IV, 64 DMT/SSB signals with 16-QAM subcarrier modulation have been generated in MATLAB and passed through the modelled architecture in VPI Photonics, before being sent to the receive function in MATLAB for digital processing. For model validation, a comparison between measured and modelled average EVM (% rms) of all signals in the multiplex versus the MZM bias voltage is shown in Fig. 11.

Note that the experimental work generally used a bias of 5.5 V, where the match between simulation and experiment is particularly good.

Further experiments have been carried out with mixed bandwidth signals by combining two different signal sets (produced from two different single-IFFT stages), employing different 5G numerologies (using the process described in Fig. 5). Specifically, the combining process was carried out in the digital domain and the composite multiplex was output from one RF port of the AWG. These results do not consider mmW up-conversion. The two signal sets have been multiplexed by mapping one signal from each numerology to each NZ, resulting in two signals (a signal group) per NZ. It should be noted that even though signals employing the same numerology can be mapped within one NZ

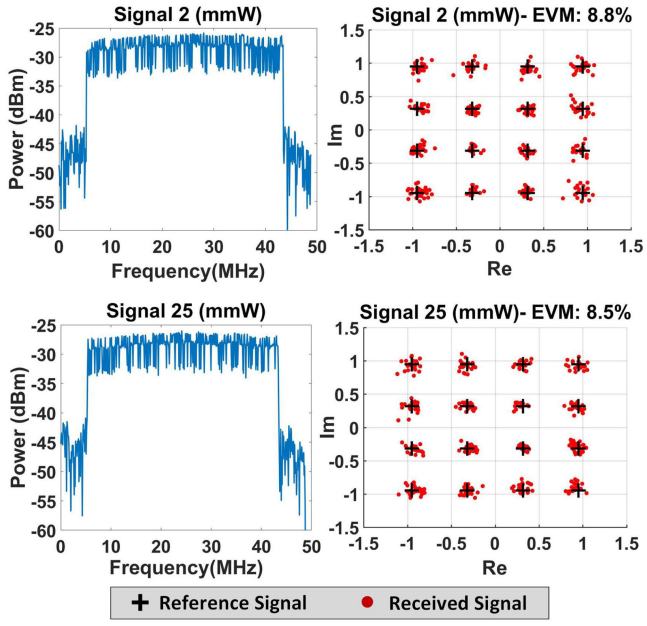

Fig. 10. Received spectra and EVM/ constellation diagrams of down-converted Signals 2 (top) and 25 (bottom) following de-multiplexing, down-sampling and up-conversion to the same mmW frequency at the RRU.

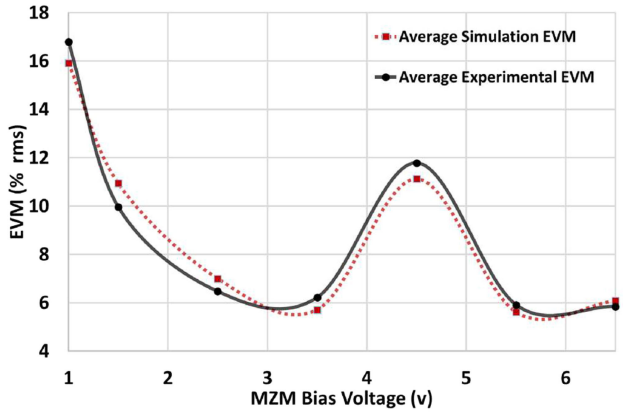

Fig. 11. Experimental and modelled MZM bias sweeps versus average EVM (% rms) for all signals (RF only).

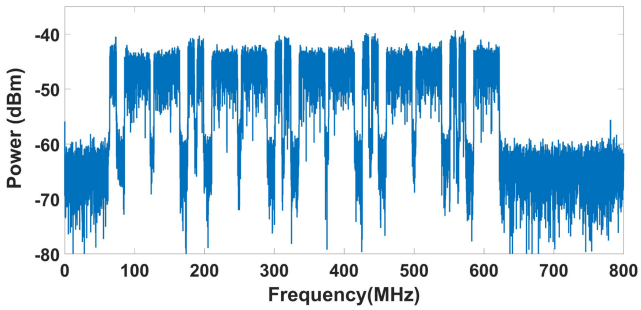

Fig. 12. Received 36-signal multiplex with mixed bandwidth signals employing 5G numerology (positive side of spectrum).

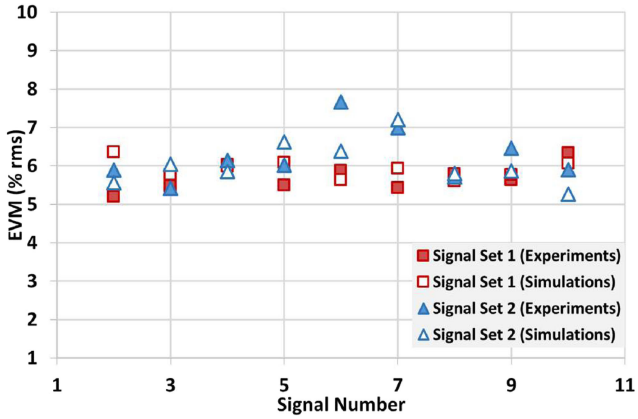

Fig. 13. Experimental and modelled EVM (% rms) of signals in Signal Sets 1 and 2, employing 5G numerologies (positive side of spectrum).

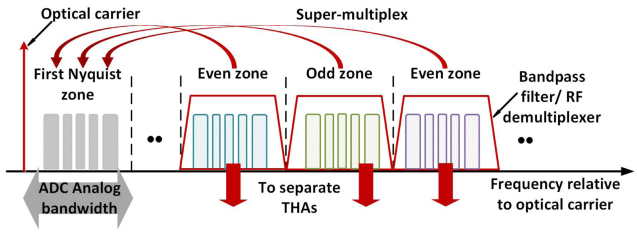

Fig. 14. Extending to a mapping hierarchy with super-multiplexes by employing a small number (dependent on ADC specifications and for practical mMIMO applications) of analog filters with multiple THAs for very large aggregate bandwidths.

(albeit at different IFs), we are using two different numerologies to demonstrate a general use case.

Signals employing the first numerology (Signal Set 1) are made up of 600 data subcarriers each (corresponding to an IFFT length of 1024) while signals of the second numerology (Signal Set 2) are made up of 300 data subcarriers each (corresponding to an IFFT length of 512). Appropriate gaps in the frequency domain are created to combine the two signal sets, resulting in a total of 36 signals (18 from each set).

Signal Set 1 has a sampling rate of 3.13 GSps while Signal Set 2 has a sampling rate of 1.56 GSps. Since the oscilloscope allows only particular sampling rates, a non-power of 2 IFFT length of 51200 has been used for both sets of signals to obtain 5G frequency bin sizes, i.e., 60 kHz for Signal Set 1 and 30 kHz for Signal Set 2. As a result, the bandwidths for the two signal sets are approximately 40 MHz and 10 MHz respectively. The resulting aggregate data rate is 3.3 Gbps (for SSB modulation). Fig. 12 shows the positive-sided spectra of the received signals from the oscilloscope. The ability to multiplex signals using this technique in a spectrally efficient manner is demonstrated by the narrow gaps between the signals: 11.8 MHz between a wide bandwidth and narrow bandwidth signal, 5.3 MHz between two wide bandwidth signals and 3.7 MHz between two narrow bandwidth signals.

Fig. 13 shows an EVM comparison between measured and simulated results for the two signal sets respectively. The EVMs for Signal Set 1 in simulations and experiments are between 5–6.5% while the EVMs for Signal Set 2 are between 5–8%. The measured and simulated EVMs for both signal sets are very close on average, and well within specification limits. Signal Set 2 has worse EVM performance, as it has slightly lower transmit power compared to Signal Set 1.

A. Use of THA in the Receiver Chain and Extension to a Mapping Hierarchy

Receiving even larger multiplexes in the manner described, would ultimately require an RRU ADC with a large analog bandwidth and sampling rate. This will happen for cases in which

- multiplexes are of aggregate bandwidths exceeding the ADC's sampling rate specifications.
- multiplexes occupy sufficiently low aggregate bandwidths but are placed at an RF such that their highest frequency component exceeds the ADC's analog bandwidth. Note that flexibility in the RF placement of the multiplex can be beneficial in certain optical network scenarios [23], [24].

Moreover, both of these conditions may be present at the same time. Such cases, as well as a technique to mitigate them using a THA, are depicted conceptually in Fig. 14.

The THA samples the received multiplex but does not quantize it. The resulting discrete-time signal is quantized by the ADC stage that follows. Larger bandwidth multiplexes are broken up into smaller blocks, e.g., 4 blocks of 32 or 64 signals each. These multiplexes are termed "super-multiplexes" as they lead

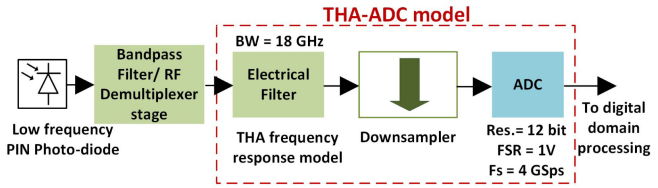

Fig. 15. Modeled frontend section of the RRU. The THA frequency response is modeled with an electrical filter prior to the down-sampler stage.

to a mapping hierarchy. Now, instead of mapping individual signals or signal groups into Nyquist zones, at the transmitter, entire multiplexes are first mapped into Nyquist zones dependent on the sampling rates of the THA and front-end ADC at the receiver. As before, signal blocks that are mapped in even Nyquist zones are frequency domain flipped and conjugated. At the receiver, each of these signal blocks is filtered using analog filters/demultiplexers and then sent to a THA, to be down-sampled to an IF (this can be the same for all blocks). This process requires the addition of analog filters, but for a wide range of mMIMO applications, and assuming sampling rates of commercially available ADCs, the required number of filters will be small. After the first down-sampling stage, the signals are processed according to the techniques described in Sections II and III.A. Thus, THAs offer flexibility in RF placement of the multiplex and flexibility of design for the creation of even larger multiplexes (or super-multiplexes), that are not limited by ADC sampling rate and/or analog bandwidth constraints. The THA offers high frequency linearity and in effect improves the analog bandwidth of the ADC.

The combined THA-ADC stage has been modeled in VPI by an analog low-pass filter, a down-sampler and an ADC, with the main model parameters shown in Fig. 15 (extracted from [25]). This stage follows the photodetector, as in the experimental setup discussed in Section III, and an analog band-pass filter (or RF de-multiplexer stage, for multiple signal blocks). The THA has an analog bandwidth of 18 GHz while the ADC has a resolution of 12 bits, Full Scale Range (FSR) of 1V and sampling rate of 3.93 GSps.

B. Simulation Setup and Performance Predictions

The simulation model is now extended to include two THAs for two blocks of mixed bandwidth signals (i.e., a super-multiplex), to demonstrate how a very large number of signals occupying a large analog bandwidth can be down-sampled using a much smaller sampling rate at the receiver. These simulations do not consider mmW up-conversion.

A block of 60 SSB modulated signals is up-converted to a frequency of approx. 5.9 GHz. A second block of signals is up-converted to a frequency of approx. 9.8 GHz, resulting in 120 signals in total within a bandwidth of 7.86 GHz. A gap in the frequency domain is used between the two blocks to facilitate analog filtering. Each of these blocks contain 30 signals of 18 MHz bandwidth (30 kHz subcarrier spacing) and 30 more signals of 72 MHz bandwidth (60 kHz subcarrier spacing). The

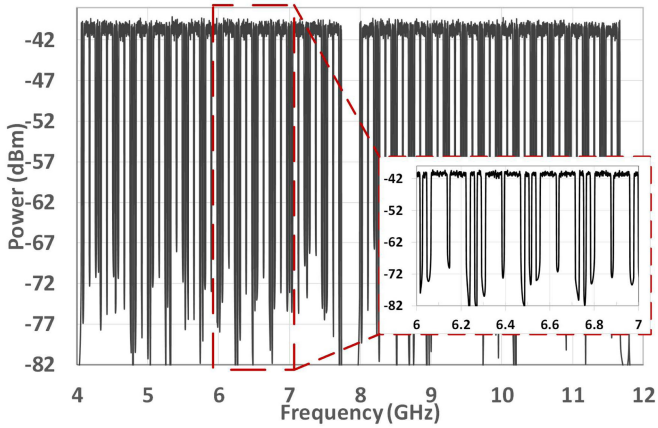

Fig. 16. 120 signal super-multiplex of mixed bandwidth signals, with 72 MHz and 18 MHz bandwidth and 30 kHz and 60 kHz subcarrier spacing (5G numerologies).

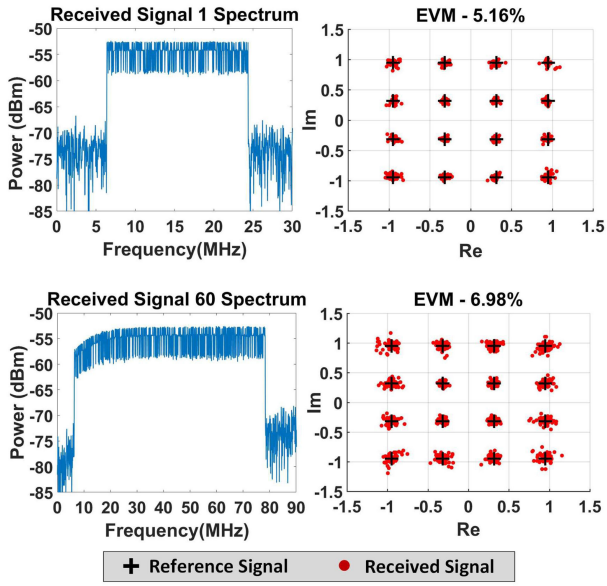

Fig. 17. Top: Received signal spectrum, EVM and constellation diagram of Signal 1 (18 MHz) of the first signal set. Bottom: Received signal spectrum, EVM and constellation diagram of Signal 60 (72 MHz) of the second signal set.

resulting multiplex is shown in Fig. 16. According to the sampling rate used at the RRU of 3.93 GSps, the first block is in an odd Nyquist zone while the second block is in an even zone and has thus been frequency domain flipped and conjugated.

At the receiver, each of these blocks is filtered and down-sampled using different THAs but with the same sampling rate of 3.93 GSps. Note that with the use of the THA the applicable frequency range of the ADC has been extended from 3.93 GHz to 18 GHz.

The down-sampled blocks are then sent to the MATLAB receive function for de-multiplexing and further processing. The received spectra, constellation diagrams and EVMs of Signal 1 of the first signal set (18 MHz bandwidth) in the first block and Signal 60 of the second signal set (72 MHz bandwidth) in the second block are shown in Fig. 17. Signal 1 is chosen as it is

the first 18 MHz signal of the 120-signal multiplex and Signal 60 is chosen as it is the last 72 MHz signal. An average EVM within the range of 5%−7% has been obtained for all signals in both signal sets in the two blocks. The aggregate data rate is 21.6 Gbps. Signals at the edge of the filter passband (e.g., Signal 60 shown in Fig. 17) show some filtering roll-off effects in their amplitude response but these can be minimized with further filtering optimization.

These results show the feasibility of extending the Nyquist zone mapping method to a hierarchical structure and thus employing receivers with arbitrarily low sampling rates and analog bandwidth specifications.

VI. Conclusion

A new and flexible mapping method for subcarrier multiplexing a large number of signals, that could be part of mMIMO and HetNet implementations, in the future 5G (and beyond) analog fronthaul has been proposed. With the use of precise Nyquist Zone mapping, the multiplexed signals can be de-aggregated and transmitted at their respective RF/mmW frequencies with minimal, per-signal digital domain processing at the RRU. Both DMT and SSB signals are multiplexed efficiently in the digital domain using a single IFFT operation-aided systematic mapping of individual signals or groups of signals into RRU-derived Nyquist Zones. Signals with different numerologies are combined by appropriate mapping within the same Nyquist zones.

In an experimental setup employing mmW up-conversion with a remotely optically delivered mmW carrier, EVM performance for a large number of multiplexed signals with generic and 5G-based numerologies, was shown to be well within LTE/5G specifications. Then, the use of track-and-hold amplifiers at the RRU, as a means of relaxing RF placement of multiplexes, and so that ever-larger "super-multiplexes" (in terms of bandwidth and/or numbers of signals) can be supported while maintaining small sampling rates and analog bandwidths at the RRU, has been proposed. Simulations show promising performance with multiple track-and-hold amplifiers, for the transport of 120 (or more, as the number can be extended for larger DU sampling rates) densely-packed signals using different 5G numerologies.

References

[1] Common Public Radio Interface (CPRI); Interface Specification, CPRI Specification V7.0, Oct. 2015. [Online]. Available: http://www.cpri.info/spec.html. Accessed on: Jan. 8, 2019.

[2] Study on New Radio Access Technology: Radio Access Architecture and Interfaces (Release 14), 3GPP Technical Specification Group Radio Access Network, TR 38.801, V14.0.0, Mar. 2017. [Online]. Available: http://www.3gpp.org/DynaReport/38-series.htm. Accessed on: Jan. 8, 2019.

[3] Common Public Radio Interface: eCPRI Interface Specification, eCPRI Specification, V1.0, Aug. 2017. [Online]. Available: http://www.cpri.info/spec.html. Accessed on: Jan. 8, 2019.

[4] N. J. Gomes, P. Assimakopoulos, M. K. Al-Hares, U. Habib, and S. Noor, "The new flexible mobile fronthaul: Digital or analog, or both?," in *Proc. Int. Conf. Transparent Opt. Netw.*, Trento, Italy, 2016, pp. 1–4.

[5] Z. Tayq *et al.*, "Real time demonstration of fronthaul transport over a mix of analogue & digital RoF," in *Proc. Int. Conf. Transparent Opt. Netw.*, Girona, Spain, 2017, pp. 1–4.

[6] X. Liu, H. Zeng, N. Chard, and F. Effenberger, "Efficient mobile fronthaul via DSP-based channel aggregation," *J. Lightw. Technol.*, vol. 34, no. 6, pp. 1556–1564, Mar. 2016.

[7] C. Browning, A. Gazman, N. Abrams, K. Bergman, and L. P. Barry, "256/64-QAM multicarrier analog radio-over-fiber modulation using a linear differential drive silicon Mach-Zehnder modulator," in *Proc. IEEE Int. Topical Meeting Microw. Photon.*, Toulouse, France, 2018, pp. 1–4.

[8] R. Hui, B. Zhu, R. Huang, C. T. Allen, K. R. Demarest, and D. Richards, "Subcarrier multiplexing for high-speed optical transmission," *J. Lightw. Technol.*, vol. 20, no. 3, pp. 417–427, Mar. 2002.

[9] R. Hui, K. Kaje, and A. Fumagalli, "Digital-analog hybrid SCM for fine-granularity circuit-switched optical networks," in *Proc. Int. Conf. Transparent Opt. Netw.*, Trento, Italy, 2016, pp. 1–7.

[10] P. Assimakopoulos, A. Nkansah, N. J. Gomes, and D. Wake, "Multichannel signal transmission through radio over fiber architecture," in *Proc. IEEE Global Commun. Conf.*, Houston, TX, USA, 2011, pp. 152–156.

[11] C. P. Liu and A. Seeds, "Transmission of wireless MIMO-type signals over a single optical fiber without WDM," *IEEE Trans. Microw. Theory Techn.*, vol. 58, no. 11, pp. 3094–3102, Nov. 2010.

[12] Z. Dong, H. Chien, and J. Yu, "Bandwidth-efficient modulation for hybrid 10G/100G optical communication networks," *IEEE Photon. Technol. Lett.*, vol. 28, no. 4, pp. 469–472, Feb. 2016.

[13] P. Torres-Ferrera, S. Straullu, S. Abrate, and R. Gaudino, "Upstream and downstream analysis of an optical fronthaul system based on DSP-assisted channel aggregation," *IEEE/OSA J. Opt. Commun. Netw.*, vol. 9, no. 12, pp. 1191–1201, Dec. 2017.

[14] R. G. Vaughan, N. L. Scott, and D. R. White, "The theory of bandpass sampling," *IEEE Trans. Signal Process.*, vol. 39, no. 9, pp. 1973–1984, Sep. 1991.

[15] L. Cheng, X. Liu, N. Chard, F. Effenberger, and G. Chang, "Experimental demonstration of sub-Nyquist sampling for bandwidth-and-hardware-efficient mobile fronthaul supporting 128x128 MIMO with 100 MHz OFDM signals," in *Proc. Opt. Fiber Commun. Conf.*, Anaheim, CA, USA, 2016, pp. 1–3.

[16] Y. Yang, C. Lim, and A. Nirmalathas, "A full-duplex digitized RoF system for millimeter-wave OFDM transmission," in *Proc. 38th Eur. Conf. Exhib. Opt. Commun.*, Amsterdam, The Netherlands, 2012, pp. 1–3.

[17] Y. Yang, C. Lim, and A. Nirmalathas, "Investigation on transport schemes for efficient high-frequency broadband OFDM transmission in fibre-wireless links," *J. Lightw. Technol.*, vol. 32, no. 2, pp. 267–274, Jan. 2014.

[18] K. A. Mekonnen, E. Tangdiongga, and T. Koonen, "High-capacity dynamic indoor all-optical-wireless communication system backed up with millimeter-wave radio techniques," *J. Lightw. Technol.*, vol. 36, no. 19, pp. 4460–4467, Oct. 2018.

[19] J. Vucic, C. Kottke, S. Nerreter, K. Langer, and W. J. Walewski, "513 Mbit/s visible light communications link based on DMT-modulation of a white LED," *J. Lightw. Technol.*, vol. 28, no. 24, pp. 3512–3518, Dec. 2010.

[20] Y. Yang, C. Lim, and A. Nirmalathas, "Bandwidth Improvement of digitized RoF system using track-and-hold amplifier" in *Proc. IEEE Int. Topical Meeting Microw. Photon.*, Noordwijk, The Netherlands, 2012, pp. 115–118.

[21] Tektronix, "Understanding AWG70000A Series Frequency Response and DAC Performance," Application Note. 2013. [Online]. Available: https://www.tek.com/document/application-note/understanding-awg70000a-series-frequency-response-and-dac-performance. Accessed on: Jan. 8, 2019.

[22] Base Station (BS) radio transmission and reception (Release 15), 3GPP Technical Specification Group Radio Access Network; NR, TS 38.104, V15.0.0. Dec. 2017. [Online]. Available: http://www.3gpp.org/DynaReport/38-series.htm. Accessed on: Jan. 8, 2019.

[23] G. Vedala, M. A. Hameed, and R. Hui, "Digital compensation of SSBI in direct detection multicarrier system with SOA nonlinearities," *IEEE Photon. Technol. Lett.*, vol. 29, no. 4, pp. 369–372, Feb. 2017.

[24] M. Xu *et al.*, "Bidirectional fiber-wireless access technology for 5G mobile spectral aggregation and cell densification," *IEEE/OSA J. Opt. Commun. Netw.*, vol. 8, no. 12, pp. 104–110, Dec. 2016.

[25] Analog Devices, "HMC1061LC5 DC – 18 GHz, ultra-wideband, dual rank 4 GS/s track-and-hold amplifier," Datasheet, Feb. 2017. [Online]. Available: http://www.analog.com/media/en/technical-documentation/data-sheets/hmc1061.pdf. Accessed on: Jan. 8, 2019.

Shabnam Noor (S'16) received the B.Sc. degree in electronics and communication engineering from BRAC University, Dhaka, Bangladesh, in 2011, and the M.Eng. degree in telecommunications from American International University-Bangladesh, Dhaka, Bangladesh, in 2013. She is currently working toward the Ph.D. degree in electronic engineering at the Communications Research Group, University of Kent, Canterbury, U.K.

She has participated in the RAPID 5G European Union-Japan Horizon 2020 research project. Her research interests include low-cost Radio over Fiber and multiplexing techniques for 5G fronthaul.

Philippos Assimakopoulos (S'09–M'16) received the B.Eng. degree in electronic engineering from the University of Bath, Bath, U.K., in 2003, and the M.Sc. degree in broadband and mobile communication networks and Ph.D. degree in electronic engineering from the University of Kent, Canterbury, U.K., in 2007 and 2012, respectively.

He is currently with the Communications Research Group, University of Kent. He has participated in various EU FP7, Horizon 2020, and UK EPSRC research projects His research interests include distributed antenna systems and low-cost microwave Radio-over-Fiber networks for indoor and outdoor applications and the design of cloud-radio access network for 4G and 5G applications.

Nathan J. Gomes (M'92–SM'06) received the B.Sc. degree from the University of Sussex, Sussex, U.K., in 1984, and the Ph.D. degree from University College London, London, U.K., in 1988, both in electronic engineering.

From 1988 to 1989, he held a Royal Society European Exchange Fellowship with ENST, Paris, France. Since late 1989, he has been with the University of Kent, Canterbury, U.K., where he is currently a Professor of optical fibre communications. His current research interests include fiber-wireless access systems and networks, fronthaul and radio-over-fiber technology.

Prof. Gomes was the TPC Chair for IEEE International Conference on Communications, ICC 2015 in London.